Main Manuscript for

Molecular Bonsai: Elucidating the design principles for engineering plant organ size.

Tawni Bull[1], Jared Van Blair[1], Sam Sutton[1], Hadley Colwell[1], Arjun Khakhar[1]

Department of Biology, Colorado State University, Fort Collins, CO[1]

Email: Arjun.Khakhar@colostate.edu

Author Contributions: T.B. and A.K. designed the research. T.B., J.V.B., S.S., and H.C. performed the experiments. T.B. and A.K. wrote the manuscript.

Competing Interest Statement: The authors declare no conflict of interest.

Classification: Plant synthetic biology.

Keywords: Gibberellin, GID1, DELLA, Modelling, Synthetic transcription factors, organ size, synthetic biology

This PDF file includes:

Main Text
Figures 1 to 6
Tables 1 to 4

Abstract

Enhancements to crop morphology, such as the semi-dwarfing that helped drive the green revolution, are often driven by changes in gene dosage. These changes are challenging to translate across varieties and species, which slows the pace of crop improvement. Synthetic transcription factors (SynTFs) offer a rapid alternative to generate targeted alterations to gene dosage. However, the complexity of developmental pathways makes it unclear how to best apply them to predictably engineer morphology. In this work, we explore if mathematical modeling can guide SynTF-based expression modulation of genes in the signaling pathway of the phytohormone, gibberellin (GA), which is a central regulator of cell expansion, to elucidate the design principles for engineering organ size. We demonstrate that modulation of GA signaling gene expression can generate consistent dwarfing across tissues in both controlled and variable environments in the model plant *Arabidopsis thaliana*, and that the degree of dwarfing is dependent on the strength of regulation as predicted by modeling. We further validate the model's predictive power by demonstrating its capacity to accurately predict the qualitative impacts of different regulatory architectures for both increasing and decreasing organ size. Finally, we show that these insights can be generalized for engineering organ size in the crop *Solanum lycopersicum* (tomato). This work creates a framework for predictable engineering of an agriculturally important trait, organ size, across tissues and plant species. It also serves as a proof-of-concept for how mathematical models can guide SynTF-based alterations in gene dosage to enable bottom-up design of plant phenotypes.

Significance Statement

While traditional breeding approaches have identified mutations that enhance crop performance via targeted gene dosage changes, these are not easily translated across varieties and species. Synthetic transcription factors (SynTFs) offer an avenue to generate such changes *de novo*, but the optimal regulatory architectures necessary to generate desired phenotypes remains unclear. We demonstrate how mathematical models can be used to guide SynTF deployment and elucidate the design principles for engineering organ size, an agriculturally important trait, via modulation of gibberellin signaling. In addition to revealing regulatory architectures that can consistently increase or decrease organ size across a range of tissues, environments, and plant species, this work demonstrates how model-guided SynTF-based modulation of gene dosage can be used to predictably engineer plants.

Main Text

Introduction

Morphological alterations, such as changes to organ size, make up a large fraction of crop trait improvements that have been selected over the course of domestication. For example, semi-dwarfed stems in cereals dramatically increased yields during the Green

Revolution by both enhancing resilience to wind damage, as well as improving productivity per unit area by enabling higher density planting (1) . Studies into the genetic basis of these improved morphologies reveal that the majority are generated by *cis*-regulatory changes that alter gene dosage (2–9). However, translating these insights to optimize traits, or introducing them into new varieties or species, using traditional breeding strategies is challenging due to epistasis, cross regulation, and an incomplete understanding of plant *cis* regulation. This necessitates trait optimization in each new genetic background, which significantly slows crop enhancement. There is an urgent need to accelerate this process to address the challenges posed by climate change and increasing demand to future food security.

The bottom-up generation of gene dosage changes using synthetic control systems represents a faster alternative for crop improvement (**Fig. 1**). Cas9-based synthetic transcription factors (SynTFs) have been demonstrated to enable layering of additional regulation on endogenous loci in plants to achieve predictable gene dosage changes (10, 11). They are also orthogonal to native developmental pathways, reducing challenges to translation across genetic backgrounds and species. This makes them an ideal tool for modulating the expression of genes to engineer phenotypes, such as organ size. However, design principles for organ size engineering with SynTFs remain opaque due to many open questions. These include which gene(s) can be modulated to generate robust and predictable changes in organ size, what the dose dependency between gene expression and phenotype is, and whether utilizing SynTFS can both increase and decrease organ size. It is also unclear whether this approach would generate consistent phenotypic changes across tissues, environments, and species.

Prior studies have revealed that the signaling pathway of the phytohormone gibberellin (GA) is a core determinant of cell expansion, and hence organ size, across plant species (3, 12–14). GA associates with its receptor, GID1 (GIBBERELLIN INSENSITIVE DWARF 1), which triggers association of GID1 and a family of transcriptional modulators, called DELLA proteins, leading to their ubiquitination and subsequent proteasomal degradation (15–17). These DELLA proteins act as negative regulators of cell expansion, and so increases in GA tend to increase organ size (15, 18, 19). Additionally, it has been shown that DELLAs are also responsible for implementing multiple transcriptional feedback loops that maintain GA homeostasis via repression of their own expression and activation of both *GID1* as well as GA biosynthesis gene (GA20 oxidases, GA3 oxidases) expression (20). This feedback combined with the presence of multiple redundant copies of these genes with differential expression patterns across tissues, makes it challenging to determine which genes in the GA signaling pathway would be ideal to regulate with SynTFs in order to generate significant changes in DELLA protein levels, and hence organ size.

A mathematical model of this feedback network parameterized using data from roots of *A. thaliana* GA signaling mutants (20) provides an avenue to qualitatively predict the impact of altering the expression of genes in the network on DELLA protein concentration. However, its predictive power remains unexplored in tissues besides roots

and in other plant species. Additionally, existing studies that use such models to guide modulation of GA regulated growth have focused on GA biosynthesis genes in the root (21–24). Studies of the role of GA signaling genes, namely *GID1* and *DELLA*, in controlling organ size have largely focused on knockout mutants or transgene overexpression. These approaches create extreme expression changes and disrupt spatiotemporal expression patterns, making it challenging to interrogate the impact of gene dosage (25–34). Thus, it remains unknown whether the expression of GA signaling genes can be modulated to predictably engineer organ size.

In this work we seek to elucidate the design principles for SynTF-based organ size engineering via modulation of GA signaling gene expression. Specifically, we explore whether mathematical models can elucidate regulatory architectures that generate robust and qualitatively predictable changes in organ size (**Fig. 1**). This includes comparing the relative efficacy of regulatory architectures for both decreasing and increasing organ size, as well as characterizing the relationship between regulation strength and phenotype to determine if it can be tuned in a dose-dependent manner. We also test whether these circuits can generate consistent organ size changes across different tissues, and if they are functional in fluctuating environments. Finally, we test whether the insights gained from the model in *A. thaliana* can be generalized to engineer organ size in an agriculturally important crop, *Solanum lycopersicum* (tomato).

Results

Model-guided repression of *GID1* generates predicted dwarfing in roots.

We implemented a modified version of a published ordinary differential equation-based model of the GA signaling network (35) to simulate the impact of SynTF-based repression of *GID1* expression on DELLA protein levels in the context of DELLA-mediated transcriptional feedback. Additional terms were added to the model to simulate SynTF expression and repression of *GID1* using a Hill equation, as described in the method section. Because DELLA has been shown to inhibit cell expansion via regulation of downstream transcription factors (TFs) (36), we used the reciprocal of DELLA protein concentration as a qualitative metric of predicted organ size. We hypothesize that this kind of linear relationship between DELLA concentration and organ size would likely not apply to very high DELLA concentrations, where the TFs that it regulates are saturated, or very low concentrations, where DELLAs would preferentially interact with the subset of TFs that have the strongest interaction strengths. However, we reasoned that this assumption should be reasonable for the moderate dosage differences from wildtype levels typically generated by SynTFs (23, 37). Our simulations predicted that the repression of *GID1* expression would reduce organ size. They also predicted that the strength of repression of *GID1* expression would be correlated with the reduction in organ size over a range of regulation strengths (**Fig. 2A**). Based on these predictions, we built *A. thaliana* transgenic lines with SynTFs targeted to regulate this gene family.

We utilized a SynTF design that enables flexible implementation of activation, repression, or editing across multiple genes *in planta* (23). It consists of a constitutively

expressed nuclease active Cas9 and RNA-binding proteins, PCP and MCP, fused to previously validated transcriptional effector domains, specifically truncations of the TOPLESS repressor for repression and the DREB2A trans-activator for activation (**Fig. 2B**). When these components are co-expressed with a guide RNA scaffold (gRNA) they enable assembly of the desired transcription factor at the promoter of the target gene (10). The gRNAs have a truncated target site, which programs Cas9 to bind rather than cut DNA (38), and motifs at their 3' end to recruit the appropriate RNA-binding protein-transcriptional effector fusion (39). Multiple transgenic *A. thaliana* lines expressing the SynTF components as well as gRNAs that assembled a repressor at the promoters of the three paralogs in the *GID1* gene family (*GID1a*, *GID1b*, and *GID1c*) were generated (10). Additionally, we generated *A. thaliana* lines that expressed all the SynTF components but no gRNAs as controls to account for the impact of selection and SynTF expression on phenotype.

Seedlings of both *GID1* repression and no gRNA control lines were grown in tandem on MS agarose plates for eight days. We subsequently measured primary root length as this was the tissue for which the model was originally parameterized. Four out of five *GID1* repression lines assessed showed significant reduction in root length when compared to a population of no gRNA control lines (**Fig. 2C**). We observed a range of root dwarfing levels in these lines, spanning a 0.41-to-0.81-fold change in median root length compared to the no gRNA control population. Based on our simulations, we hypothesized that this variation in phenotype strength was due to the expected variation in the strength of *GID1* repression across independent transgenic events associated with random insertion and copy number variation of SynTF components.

To test this hypothesis, we conducted RT-qPCR to measure the degree of *GID1* repression across these lines. We observed significant *GID1a* and *GID1c* repression across lines compared to the no gRNA controls (**Fig. 2D and 2E**). However, no *GID1b* repression was observed in any line (**Fig. S1A**). We hypothesize this is due to an inefficient gRNA target sequence. We then measured the correlation between tandem measurements of *GID1* expression and root length and observed significant positive correlations for *GID1a* (R^2 = 0.55) and *GID1c* (R^2 = 0.55) (**Fig. S1C,D**). We observe an even stronger correlation (R^2 = 0.63) between the total *GID1a* and *GID1c* expression in the plant and root length, which is consistent with these genes being functionally redundant (**Fig. 2F**). These results are consistent with model predictions showing that increasing SynTF repression of *GID1* would increase DELLA protein levels, leading to larger reductions in organ size (**Fig. 2A**). We also noted that the *GID1* repression was most visible in tissues sampled at night, but non-significant in tissues collected in the day (**Fig. S1B**). This is consistent with the reported circadian oscillation of *GID1* expression, with low expression in the day making repression challenging to observe and high expression at night revealing the impact of

SynTF-based repression (40). Taken together, these results validate *GID1* as a good target for SynTF-based engineering of root dwarfing.

SynTF-based repression of *GID1* results in smaller organ size across multiple tissues.

As the parametrization of the model that predicted *GID1* repression would lead to dwarfing was based on data collected from *A. thaliana* seedling roots, it was possible that this circuit would not generate the same phenotype across other tissues and developmental times (20). To explore this, we measured shoot phenotypes at different developmental times, including hypocotyl length and leaf size, in a subset of the transgenic lines with SynTF-based repression of *GID1* described above.

Prior work has demonstrated that the GA signaling pathway plays a major role in hypocotyl elongation (14, 41, 42). Based on this work, if the model predicted an increase in DELLA concentration upon *GID1* repression, we would expect a decreased ability for hypocotyl elongation. To test this hypothesis, we instigated hypocotyl etiolation in newly germinated seedlings of *GID1* repression lines in tandem with no gRNA controls lines via incubation in the dark on MS agar plates. We observed that the *GID1* repression lines that were tested showed a significant decrease in hypocotyl length when compared to the no gRNA control population (**Fig. 3B**). We also observed a strong correlation (R^2 = 0.68) between the strength of dwarfing, quantified as the fold change in organ size compared to the no gRNA controls, observed in roots and hypocotyls across these lines (**Fig. 3C,J**). These observations further validate the role played by GA signaling in hypocotyl elongation (14, 41) and demonstrate the capacity of SynTF-based *GID1* repression to generate consistent dwarfing across tissues.

We also measured individual leaf area and calculated total rosette size in *GID1* repression lines and observed a significant decrease in both phenotypes compared to the no guide control population (**Fig. 3H,I**). Like our measurements of hypocotyl length, lines with the strongest dwarfing in roots had the largest changes in rosette size (**Fig. 3H**). These results, in conjunction with the correlation between *GID1* expression and root length (**Fig. 2F**), show that repressing *GID1* expression generates a consistent degree of dwarfing across tissues that is dependent on the strength of regulation.

Interestingly, we observed that in the distribution of leaf areas across developmental time, the lower bound of the distribution is not decreased in the GID1 repression lines when compared to the control but the upper bound is, driving an overall decrease in leaf area (**Fig. 3F,G,I**). These observations are consistent with the previously reported phenotypes of knockouts of GID1 (15) and with our hypothesized reduction in cell expansion in the GID1 repression lines compared to the no guide control lines. The invariant lower bound in leaf size is due to processes inherent to leaf development wherein cells transition from a phase of mainly cell division, where lines behave similarly, to cell expansion (43), where GID1 repression lines are unable to expand as much as control lines. Taken together, these results demonstrate that SynTF-based repression of

GID1 reduces organ size consistently and in a dose-dependent manner across a range of tissues and developmental times.

Reductions in organ size generated by SynTF-based repression of *GID1* are stable across fluctuating environments.

Thus far all our phenotyping has been conducted in controlled growth conditions to minimize the potentially confounding impact of variable environments on GA signaling (28) . However, as we hope to eventually use these tools to design crops that are grown in field conditions, it is important to test if the dwarfing generated by SynTF-based repression of *GID1* is stable in fluctuating environmental conditions. For these experiments, three *GID1* repression lines that showed a range of dwarfing strengths in prior experiments and the no gRNA control population were grown in tandem in a greenhouse without any active temperature or light control. We measured these plants for their inflorescence height due to the ease of measurement of this phenotype in greenhouse grown plants and reports from previous studies demonstrating *GID1* knockouts show reductions in inflorescence height (15).

Multiple inflorescence phenotypes were observed in the *GID1* repression lines when compared to the no gRNA control lines. Upon phenotyping, we noted a significant delay in the bolting of *GID1* repression lines compared to the no gRNA control lines (**Fig. 3K**), which is consistent with an increased DELLA protein concentration. This provides secondary evidence beyond the dwarfing that the modulation of GID1 is leading to the predicted changes in DELLA protein levels. To prevent differential bolting times from confounding the assessment of inflorescence height, the height was measured once all plants had bolted and was normalized by the number of days post bolting. We observed a significant reduction in inflorescence height in *GID1* repression lines compared to no guide control lines (**Fig. 3L**), as predicted. Additionally, the relative strength of dwarfing observed across these lines was consistent with what was observed across experiments in more controlled conditions. These results show that SynTF-based repression of *GID1* can generate dwarfing phenotypes that are both consistent across a range of tissues and resilient to fluctuating environments.

Activating *DELLA* expression generates similar phenotypes to repressing *GID1*

We next used our model of GA-signaling in the root to interrogate how SynTF-based activation of *DELLA* expression would alter DELLA protein levels in the context of its negative transcriptional feedback. Simulations predicted that the activation of *DELLA* expression would result in higher DELLA protein concentrations and hence a reduction in organ size, i.e. root length, and that the strength of dwarfing would depend on regulation strength (**Fig. 4A**). To test this prediction, we built transgenic *A. thaliana* lines expressing the same SynTF components as used in the *GID1* repression lines as well as gRNAs that were designed to assemble an activator at the promoters of each of the five *DELLA* genes

in *A. thaliana*, namely REPRESSOR OF GA (*RGA*), GIBBERELLIC ACID INSENSITIVE (*GAI*), RGA-LIKE 1 (*RGL1*), RGA-LIKE 2 (*RGL2*), and RGA-LIKE 3 (*RGL3*) (**Fig. 4B**).

The primary root lengths of eight-day-old transgenic lines were measured and compared to the same population of no gRNA control lines as described earlier. Of the six independent lines tested, five showed a significant reduction in primary root length compared to controls, spanning a 0.2-to-0.56-fold change, which is consistent with model predictions (**Fig. 4C**). We also observed a significantly higher expression of the two major *DELLAs* targeted by the SynTF, *RGA* and *GAI*, in a line with stronger dwarfing compared to a line with weaker dwarfing (**Fig. S2A,B**). This validates the model's prediction that the degree of dwarfing is dependent on SynTF regulation strength. Additionally, when we compared the fold change in root length of all the *DELLA* activation lines to that of all the *GID1* repression lines we observed no significant difference in the overall dwarfing generated by these two regulatory architectures (**Fig. S2C**). Taken together, these results demonstrate that activating *DELLA* is a viable alternative to repressing *GID1* for controlling root organ size.

SynTF-based modulation of *GID1* or *DELLA* expression enables increasing organ size

In the experiments described thus far we have utilized model-guided reprogramming of GA-signaling gene expression to decrease organ size. However, in some contexts it might be useful to increase organ size, for example increasing fruit size to improve yields or increasing root network size to enable drought resilience. We next explored whether modulating the expression of *GID1* and *DELLA* in the opposite way, i.e., activation of *GID1* expression and repression of *DELLA* expression, can generate organ size increases. We used a modified version of the model described above, with terms for either SynTF-based activation of *GID1* expression or repression of *DELLA* expression, to simulate the DELLA protein concentration at steady state for a range of different SynTF regulation strengths. The model predicted both regulatory architectures would lead to lower concentrations of DELLA protein, and hence an increase in organ size, compared to the no gRNA control (**Fig 5D,G**). The magnitude of organ size increase was predicted to be proportional to the strength of regulation. Interestingly, *GID1* activation is predicted to result in both a smaller linear range in organ size across SynTF regulation strengths, with an earlier saturation, as well as a lower magnitude of organ size increase than *DELLA* repression (**Fig 5D,G, S3C**).

To test these predictions, we generated transgenic *A. thaliana* lines expressing the same SynTF components discussed above as well as gRNAs targeting either the three *GID1s* for activation or the five *DELLA*s for repression (**Fig. 5A**). Six independent lines of each genotype were then grown in tandem with no gRNA control lines on MS agar plates and hypocotyl length was measured as described above. In tandem, we also collected RNA from a subset of these lines and measured expression of the target genes. Specifically, we measured *GID1a* and *GID1c* in the *GID1* activation lines, as these were found to drive the phenotype in the *GID1* repression lines described previously. In the *DELLA* activation lines we measured the expression of the two major DELLAs, RGA and

GAI. We observed significant activation of *GID1a* and *GID1c* (**Fig 5B**), as well as significant repression of *RGA* and *GAI* (**Fig 5C**) compared to the no gRNA controls across multiple lines. We also observed that all lines tested from both regulatory architectures resulted in a significant increase in hypocotyl length compared to the no gRNA controls with a range of phenotype strengths, as predicted by the model (**Fig 5D-I**). When we compared the total *GID1* or *DELLA* expression measured with the fold change in hypocotyl length across lines that spanned the range of observed phenotypes, we observed a strong correlation (*GID1* activation R^2=0.96, *DELLA* repression R^2=0.76) validating the predicted relationship between regulation strength and organ size (**Fig S3A,B**).

The model's prediction that *GID1* activation would lead to a smaller linear range in organ size compared to *DELLA* repression is evident from comparing the average hypocotyl length across the six lines of each genotype (**Fig 5F,I**). We observe a significantly smaller range of hypocotyl length across the *GID1* activation lines (~0.1 cm) compared to *DELLA* repression lines (~0.32 cm). To test the model's prediction that *DELLA* repression would also generate a larger magnitude of organ size increase than *GID1* activation (**Fig 5L**), we compared the fold change in hypocotyl length of the lines with the strongest phenotypes. We observed a significantly higher fold change in hypocotyl length compared to the no gRNA control for *DELLA* repression (0.96) compared to *GID1* activation (0.29). These results demonstrate that while increasing organ size is possible via modulation of both *GID1* and *DELLA* expression, *DELLA* repression can generate a stronger phenotype than *GID1* activation.

Finally, to further test the qualitative predictive power of the model, we used it to interrogate the relative impact on organ size of different regulatory architectures. The model predicted that *DELLA* repression would generate a larger magnitude organ size change compared to *DELLA* activation (**Fig 5J**). We compared the fold change in hypocotyl length compared to the no gRNA controls in the line with the strongest phenotype for both genotypes and observed that this prediction was validated, with the mean fold change of the *DELLA* repression and *DELLA* activation lines being 0.47 and 0.33, respectively (**Fig 5K**). Similarly, the model predicted that *GID1* repression would generate a larger change in organ size than *GID1* activation (**Fig S3D**), and we observed a 0.37- and 0.27-fold change compared to the no gRNA controls for the strongest *GID1* repression and *GID1* activation lines, respectively (**Fig S3E**). These results demonstrate the utility of model-guided deployment of SynTF-based expression reprogramming for engineering morphology.

SynTF-based repression of *GID1s* can generate expected phenotypes in tomato

Our results thus far demonstrate that model-guided SynTF-based expression reprogramming of GA-signaling genes enables predictable modulation of organ size in the model species, *A. thaliana*. However, as the goal of this work is to elucidate the design rules for engineering organ size in crops, we next explored whether these principles could be generalized to a major crop plant *Solanum lycopersicum* (tomato). Specifically, we focused on testing whether SynTF-based repression of *GID1* could generate robust

reduction in organ size across the root and shoot tissues in tomato as such compact morphologies have the potential to increase yields in indoor growth environments where space is at a premium (44) . We generated transgenic tomato lines with a single protein SynTF, consisting of a nuclear localized deactivated Cas9 fused to the N-terminal 188 amino acids of the TOPLESS repressor (37), and gRNAs targeting the promoters of the three *GID1* genes, *GID1a*, *GID1b-1*, and *GID1b-2* (**Fig. 6A**). These lines were grown in tandem with controls lacking the SynTF and the length of primary roots and hypocotyls was measured. We observed both decreased hypocotyl length and root length in the four independent *GID1* repression lines tested (**Fig. 6B,C**). Additionally, we also observed that the lines with the strongest shoot dwarfing also had the strongest root dwarfing, replicating the consistent impact across tissues. Taken together, these results demonstrate that the design principles for SynTF-based engineering of organ size can be generalized to tomato.

Discussion

Our results demonstrate that repression of the *GID1* genes with SynTFs can generate predictable and tunable dwarfing in *A. thaliana* roots. We observed that *GID1* repression generated a range of reductions in root lengths across independent lines that correlated with the strength of SynTF-implemented repression of *GID1*. This was consistent with the model's prediction that increasing strength of repression by the SynTF would result in higher DELLA protein concentrations and hence larger reductions in organ size. While prior studies had used knockouts and overexpression to elucidate the role that the *GID1* genes play in regulating cell expansion (3, 12, 13), our results are the first demonstration that titrating their expression is sufficient to generate predictable, dosage-dependent changes in organ size (**Fig. 2E**). The approach of tuning the expression of this gene family to generate changes in organ size will enable future interrogation of the relationship between organ size and physiology beyond the extremes generated by knockouts and overexpression and without confounding co-variation in other traits that can stymie studies of natural variation. Our observation that the repression implemented by SynTFs was only visible in tissues collected in the evening is consistent with the reported circadian oscillations of *GID1* expression (40) . This suggests a molecular model where, in the no guide controls the spike of *GID1* expression in the evening reduces DELLA protein levels and enables cell expansion, while in the *GID1* repression lines this spike is suppressed leading to lower cell expansion.

This work also shows that *GID1* repression enables reduction of organ size across tissues and environments. This demonstrates that the GA-signaling based control of cell expansion functions similarly across cell types and implies that SynTF-based expression reprogramming can be applied to engineer the size of a range of tissues. We also observed significant dwarfing in GID1 repression lines grown in variable greenhouse environments, which indicates that these circuits are stable in fluctuating environmental conditions. This is a critical determinant of the utility of this approach for engineering crops, which are grown in the variable field and greenhouse environments.

The comparison between the reduction in root length observed in *A. thaliana* lines with *DELLA* activation and *GID1* repression demonstrates that *DELLA* activation is a viable alternative for generating dwarfing. This is a valuable insight as the *GID1* and *DELLA* gene families have different numbers of homologs across species, for example *A. thaliana* has five DELLAs while tomato has one. Because SynTF regulation tends to become less efficient with more targets due to competition for resources, targeting the minimum number of genes is desirable for implementing strong regulation. Thus, knowing that regulation of either *DELLAs* or *GID1s* can generate equivalent dwarfing enables selecting the smallest gene family to target in a crop.

In addition to reducing organ size, our results also demonstrate that modulating expression of *GID1* and *DELLA* in the opposite direction is an avenue to increase organ size. While both *GID1* activation and *DELLA* repression generated increases in *A. thaliana* root length, we observed a significantly larger effect on organ size from *DELLA* repression overall, which was consistent with model simulations. The model also accurately predicted the larger fold change in organ size from *DELLA* repression compared to *DELLA* activation, and *GID1* repression compared to *GID1* activation, which highlights its predictive power. While these predictions remain qualitative, they demonstrate how such models can be used to identify the best regulatory architectures to achieve a target morphology. In the future, SynTF-based titration of GA-signaling gene expression in crop species will facilitate generating parametrization data for quantitatively predictive models. These will open the door to precision design of organ size using SynTFs.

Finally, the demonstration that *GID1* repression can also generate reductions in organ size across tissues in tomato implies that the design principles for engineering organ size elucidated above can be generalized across species. This is likely due to the highly conserved role GA-signaling plays in the control of cell expansion across plant species as well as the orthogonal nature of SynTF based regulation (45, 46). However, rigorous validation of this claim will require characterization of the phenotypic outcomes of these circuits across a range of monocot and dicot crop species. These results highlight the promise of utilizing model-guided SynTF-based expression engineering for bottom-up design of morphology across a range of crops in the future.

However, while promising, there are still aspects of this approach that need to be refined to achieve its full potential. While the existing systems are useful for modulating organ size, such global changes are often associated with negative pleiotropies. For example, while dwarfed stems might increase productivity and resilience, associated root dwarfing can reduce water and nitrogen use efficiency. In addition, the cross regulation of other traits by GA signaling, such as flowering time (17, 47, 48), mean global reprogramming of GA signaling could also lead to unintended consequences such as the delayed flowering we observed in our greenhouse experiments. Restricting the activity of SynTFs using tissue specific expression strategies could enable targeted changes to the size of specific organs. This highlights a potential benefit of targeting GA signaling genes, such as *GID1s* and *DELLAs*, over the strategies that have been explored thus far which focus on modulation of GA biosynthesis. As GA is actively trafficked through plant tissues

local changes could result in systemic morphological alterations. In contrast, targeting the GA signaling genes with SynTFs would sidestep these challenges as they have cell autonomous effects, thereby minimizing the chances of transport related pleiotropies.

Additionally, while this work provides a robust synthetic framework for controlling cell expansion, this is only one of several determinants of organ size, which limits the extent of morphological reprograming possible. This was demonstrated in our ability to restrict the upper bound, but not the lower bound of leaf size in *A. thaliana*. Tools for the precision control of cell division and extracellular matrix deposition will be necessary to enable wholistic bottom-up control of organ size in the future. Finally, we show that our approach can generate a range of phenotype strengths, thanks to the range of regulation strengths obtained from insertional variation of the SynTFs across transgenic events. Transitioning from this line generation and screening approach to the predictable tuning of phenotype requires two major innovations. Firstly, strategies to predictably tune the regulation strength of SynTFs and secondly, technologies such as landing pads or targeted insertion into validated safe harbors to enable consistency across transgenic events.

Enabling the bottom-up design of crop traits via precision changes to gene expression would be a step change in the process of crop enhancement. Moving from iterative phenotype-based selection of beneficial natural mutations to model guided alterations of gene dosage using SynTFs would accelerate trait engineering. Additionally, the use of SynTFs that are largely orthogonal to endogenous signaling pathways enables predictable alterations to gene expression and associated phenotypes across tissues and species, as we demonstrate. This contrasts with *cis*-regulatory variation isolated from breeding approaches that can lead to variable phenotypes across genetic backgrounds thanks to cross-regulation of pathways, epistasis and linkage drag. Finally, bottom-up design with synthetic systems would grant access to regions of biological design space that have not been sampled by natural variation due to evolutionary bottlenecks or associated negative pleiotropies.

Overall, this work advances our fundamental understanding of GA signaling, specifically the relationship between signaling gene expression and organ size. It also lays the groundwork for the bottom-up design of crop morphology by elucidating the design principles for using SynTFs, guided by mathematical models of GA signaling, to reprogram organ size. This opens the door to a range of exciting translational applications including engineering plant-based biomaterials and creating morphologies that maximize productivity in specific environments, be they fields, indoor farms, or spaceships.

Materials and Methods

Model simulations

A modified version of the mathematical model of GA signaling, originally developed by Middleton et al.(35), was implemented in python to simulate the impact of SynTF-based regulation of *GID1* or *DELLA* expression on steady state DELLA protein levels. This involved adding equations to simulate SynTF transcription (**Eq. 1**) and translation (**Eq. 2**) as well as

modifications to the Hill equations simulating *GID1* activation (**Eq. 3**) or repression (**Eq. 4**), or *DELLA* activation (**Eq. 5**) or repression (**Eq. 6**). These are shown below.

Eq. 1 – $\frac{d[SynTF_{mRNA}]}{dt} = \varphi_{SynTF_{mRNA}} * (k_{SynTF} - SynTF_{mRNA})$

Eq. 2 – $\frac{d[SynTF]}{dt} = \Delta_{SynTF} * SynTF - \mu_{SynTF} * SynTF$

Eq. 3 – $\frac{dGID1_{mRNA}}{dt} = \varphi_{GID1_{mRNA}} * (\frac{DELLA+SynTF*\theta_{SynTF}}{DELLA+\theta_{GID1_{mRNA}}+SynTF*\theta_{SynTF}} - GID1_{mRNA})$

Eq. 4 – $\frac{dGID1_{mRNA}}{dt} = \varphi_{GID1_{mRNA}} * (\frac{DELLA}{DELLA+\theta_{GID1_{mRNA}}+SynTF*\theta_{SynTF}} - GID1_{mRNA})$

Eq. 5 – $\frac{dDELLA_{mRNA}}{dt} = \varphi_{DELLA_{mRNA}} * (\frac{\theta_{DELLA_{mRNA}}+SynTF*\theta_{SynTF}}{DELLA+\theta_{DELLA_{mRNA}}+SynTF*\theta_{SynTF}} - DELLA_{mRNA})$

Eq. 6 – $\frac{dDELLA_{mRNA}}{dt} = \varphi_{DELLA_{mRNA}} * (\frac{\theta_{DELLA_{mRNA}}}{DELLA+\theta_{DELLA_{mRNA}}+SynTF*\theta_{SynTF}} - DELLA_{mRNA})$

The constants for these equations (φ-scaler for transcription, Δ-rate of translation, μ-rate of protein decay) were either kept the same as the original Middleton *et al*. model or were assumed to be the same as the DELLA for those associated with the SynTF. The values used are detailed in the associated jupyter notebook on github (https://github.com/arjunkhakhar/250610_GA_signaling_paper). For the SynTF we explored a broad range of both expression levels (k_{SynTF}) and regulation strengths (Θ_{SynTF}). To analyze steady state DELLA concentrations, we picked initial conditions where all variables were set to zero and ran a numerical solver (odeint) from the scipy package for fifty thousand timesteps at which point all variables were at, or asymptotically approaching, steady state. The steady state DELLA concentrations were then plotted using functions from the matplotlib and seaborn packages.

Plasmid construction

All plasmids constructed in this work were built using Golden Gate Assembly and Modular Cloning (49, 50) and are listed with links to their annotated plasmid maps in **Supplemental Table S1**. Codon optimized sequences of nuclease active Cas9, PCP, MCP, and TPL188 with correct restriction site overhangs were amplified from previously reported plasmids (10). The sequence for the DREB2A activation domain with restriction site overhangs was synthesized using Twist Bioscience. All sgRNA target sequences in this work were designed using CHOPCHOP v3 (51) and target sequences are listed in **Supplemental Table S2**. The gRNA sequences were added to various DNA parts as overhangs using primers and were reconstituted during the assembly and ligation process. Recruitment motif sequences, PP7 and MS2, used in this study were previously reported (10, 52). All plasmids used in this work will be available via AddGene.

Transgenic line regeneration

The *Arabidopsis thaliana* transgenic lines described in the work were generated by introducing the SynTF components and gRNAs targeting the promoters of either the *GID1s* or *DELLAs* into the genome of Col-0 via floral dip (53). Multiple independent T1 or T2 lines were used for further experiments. The transgenic tomato lines described in this work were generated via construction of a T-DNA encoding the Cas9-based repressor described in the main text as well as gRNAs to target it to the promoters of the three *GID1* genes and subsequent *Agrobacterium*-mediated transformation that was outsourced to the plant transformation center at UC Davis. The recovered transgenic lines were confirmed for SynTF expression via RT-qPCR and multiple independent T2 lines were used for subsequent experiments.

***Arabidopsis* root phenotyping**

Seeds were surface sterilized in a solution containing 70% Ethanol and 0.05% Triton-X-100 for 20 minutes. Seeds were immediately rinsed with 95% Ethanol. Seeds were plated on 1/2x MS (54) containing 0.8% PhytoAgar™ (plantmedia Cat. No. 40100072-1) and Kanamycin (50mg/L). After plating the seeds, plates were stratified in the dark at 4°C for five days. After five days, plates were grown vertically under short day conditions (9hr light/15hr dark) at 22°C in a Percival growth chamber for 8 days. Plates were scanned using an Epson scanner and root length was measured using ImageJ.

Gene expression analysis via RT-qPCR

For characterization of *GID1* and *DELLA* expression, whole eight-day-old seedlings from the root phenotyping assays of the different regulatory architectures and no gRNA control lines were harvested either during the day or one hour after dark and immediately frozen in liquid nitrogen. RNA was extracted using the QIAGEN RNeasy Plant Mini Kit (Cat No. 74904). The RNA samples were treated with the TURBO DNA-*Free*™ kit (Invitrogen Cat No. AM1907) to remove genomic DNA. Complementary DNA (cDNA) was synthesized using the LunaScript® RT SuperMix Kit. Proper removal of the genomic DNA was confirmed with PCR using GoTaq® Green Master Mix (Promega Cat No. M7122) and primers spanning the first and second intron of *GID1a*. Concentrations of *GID1a*, *GID1b*, *GID1c*, *RGA*, *GAI*, and *PP2A* were quantified using RT-qPCR performed with the Luna® Universal qPCR Master Mix on the BioRad CFX Opus qPCR machine. Cycle threshold values *GID1* and *DELLA* were normalized to the housekeeping gene (*PP2A*). Two technical replicates were performed for all samples. The PCR and RT-qPCR primers used are listed in **Supplemental Table S3.**

***Arabidopsis* shoot phenotyping**

For hypocotyl measurements, seeds of *A. thaliana* transgenic lines were surface sterilized and plated on media plates as described above. Plates were stratified for three days in the dark at 4°C, light shocked for six hours in a Percival growth chamber set to 22°C and

short-day conditions (9hr light/ 15hr dark) and then were wrapped in foil and placed vertically in the growth chamber to promote etiolation. After three days, plates were scanned using an Epson scanner and hypocotyls were measured using Image J.

For rosette and leaf phenotyping, seeds of *A. thaliana* transgenic lines were surface sterilized and plated as described above. Seeds were stratified for three days in the dark at 4°C, light shocked for six hours in a Percival growth chamber set to 22°C and long-day conditions (16hr light/8hr dark) and then were wrapped in foil and returned to the growth chamber. After three days, the foil was removed, and plates were returned to the growth chamber. After 15 days, 12 seedlings were transplanted into soil (2:1 Pro-Mix HP to Vermiculite mix) in 2.5-inch square pots and placed in a Conviron growth chamber set to 22°C, long-day conditions (16hr light/8hr dark), 150uM light intensity, and 60% relative humidity. Plants were placed in flats in a randomized block design and were bottom-watered every two to three days with tap water. After 15 days in the growth chamber, each plant was dissected by leaf and scanned in order of developmental age. Individual leaf areas were measured using ImageJ. Rosette areas were calculated by summing the areas of individual leaves for each plant.

For inflorescence phenotyping, seeds of A. thaliana transgenic lines were surface sterilized and plated on 1/2x MS media plates as described above. Plates were stratified for three days in the dark at 4°C and then transferred into Percival growth chamber set to 22°C and short-day conditions (8hr light/16hr dark). Three-week-old seedlings were transplanted into soil (2:1 Pro-Mix HP to Vermiculite mix) into 2.5-inch square pots. Plants were organized in a randomized block design in a greenhouse and bottom-watered by hand every two to three days. Plants were monitored daily and the date that individual plants transitioned to reproductive growth was collected. Once all plants had inflorescences that reached at least approximately 2 centimeters in height, inflorescence height was collected. Inflorescence height was normalized by days-post bolting for better comparisons of dwarfing between genotypes.

Tomato phenotyping and gene expression analysis

Seeds of M82 WT and *GID1* repression tomato lines were surface sterilized in 10mL of 20% commercial bleach with 2 drops of Tween20 with constant agitation for 20 minutes. Seeds were rinsed three times with sterile water. Approximately 20 seeds per line were sown in Magenta boxes containing 1/2x MS supplemented with 50ug/mL Kanamycin and placed in a Percival growth chamber set to 25°C and long day (16hr light/8hr dark) conditions. Hypocotyl and root length of 14-day old seedlings were measured and seedlings were transplanted into ProMix HP soil in 4-inch square pots.

To measure *GID1* expression in transgenic vs WT plants, tissue was collected one hour after dark by sampling whole 14-day-old seedlings. Seedlings were dissected into hypocotyls and roots and immediately frozen in liquid nitrogen. Seedling tissue was stored at -80°C prior to lysing. Cells were lysed using a mechanical tissue lyser and RNA was extracted using TRIzol (55) followed by treatment with the TURBO DNA-*Free*™ kit (Invitrogen Cat No. AM1907) to remove genomic DNA. The LunaScript® RT SuperMix Kit

was used to synthesize cDNA. Concentrations of *GID1a*, *GID1b*, *GID1b2,* and *CAC* were quantified using RT-qPCR performed with the Luna® Universal qPCR Master Mix on the BioRad CFX Opus qPCR machine. Two technical replicates were performed for all samples. The PCR and RT-qPCR primers used are listed in **Supplemental Table S3.** Cycle threshold values of the *GID1* genes were normalized to the housekeeping gene (*CAC*).

Data analysis and plotting

All data analysis was performed in python using Jupyter Lab (version 3.4.4). The p-values reported were calculated using either an ANOVA or a T-test for pairwise comparisons where appropriate using the scipy package in python. All the data that is presented was plotted using the seaborn package and functions from the matplotlib library (56) . All the raw data and code used to analyze the data is available on the following github repository (https://github.com/arjunkhakhar/250610_GA_signaling_paper).

Acknowledgments

We would like to thank Dan Voytas and Colby Starker for their help with transgenic lines and plasmids when we were setting up our lab. T.B. and J.V.B. were supported by an award from the CROPPS center. CROPPS research is conducted with major support from the National Science Foundation under Grant No. DBI-2019674. A.K. was supported in part by funding from the National Science Foundation under Grant No. 2310396.

References

1. Y. Eshed, Z. B. Lippman, Revolutions in agriculture chart a course for targeted breeding of old and new crops. *Sci New York N Y* **366**, eaax0025 (2019).

2. R. J. Cowling, N. P. Harberd, Gibberellins control Arabidopsis hypocotyl growth via regulation of cellular elongation. *J. Exp. Bot.* **50**, 1351–1357 (1999).

3. L. R. Band, *et al.*, Growth-induced hormone dilution can explain the dynamics of plant root cell elongation. *Proceedings of the National Academy of Sciences* **109**, 7577–7582 (2012).

4. C. Gallego-Giraldo, *et al.*, Role of the gibberellin receptors GID1 during fruit-set in Arabidopsis. *Plant J.* **79**, 1020–1032 (2014).

5. N. Illouz-Eliaz, *et al.*, Multiple Gibberellin Receptors Contribute to Phenotypic Stability under Changing Environments. *Plant Cell* **31**, 1506–1519 (2019).

6. N. Illouz-Eliaz, *et al.*, Mutations in the tomato gibberellin receptors suppress xylem proliferation and reduce water loss under water-deficit conditions. *J. Exp. Bot.* **71**, 3603–3612 (2020).

7. H. Suzuki, *et al.*, Differential expression and affinities of Arabidopsis gibberellin receptors can explain variation in phenotypes of multiple knock-out mutants. *Plant J* **60**, 48–55 (2009).

8. J. Doebley, A. Stec, L. Hubbard, The evolution of apical dominance in maize. *Nature* **386**, 485–488 (1997).

9. S. Hake, J. Ross-Ibarra, Genetic, evolutionary and plant breeding insights from the domestication of maize. *eLife* **4**, e05861 (2015).

10. A. Khakhar, *et al.*, ViparíNama: RNA viral vectors to rapidly elucidate the relationship between gene expression and phenotype. *Plant Physiol* 2020.06.03.130179 (2021). https://doi.org/10.1093/plphys/kiab197.

11. S. Selma, *et al.*, Strong gene activation in plants with genome-wide specificity using a new orthogonal CRISPR/Cas9-based programmable transcriptional activator. *Plant Biotechnol. J.* **17**, 1703–1705 (2019).

12. S. Chen, *et al.*, Identification and characterization of tomato gibberellin 2-oxidases (GA2oxs) and effects of fruit-specific SlGA2ox1 overexpression on fruit and seed growth and development. *Hortic Res* **3**, 16059 (2016).

13. F. N. Ritonga, *et al.*, The Roles of Gibberellins in Regulating Leaf Development. *Plants* **12**, 1243 (2023).

14. L. Ragni, *et al.*, Mobile Gibberellin Directly Stimulates Arabidopsis Hypocotyl Xylem Expansion . *Plant Cell* **23**, 1322–1336 (2011).

15. J. Griffiths, *et al.*, Genetic Characterization and Functional Analysis of the GID1 Gibberellin Receptors in Arabidopsis. *Plant Cell Online* **18**, 3399–3414 (2006).

16. M. Nakajima, *et al.*, Identification and characterization of Arabidopsis gibberellin receptors. *Plant J.* **46**, 880–889 (2006).

17. A. Dill, S. G. Thomas, J. Hu, C. M. Steber, T. Sun, The Arabidopsis F-Box Protein SLEEPY1 Targets Gibberellin Signaling Repressors for Gibberellin-Induced Degradation[W]. *Plant Cell* **16**, 1392–1405 (2004).

18. P. Achard, *et al.*, Integration of Plant Responses to Environmentally Activated Phytohormonal Signals. *Science* **311**, 91–94 (2006).

19. E. Gendreau, *et al.*, Cellular Basis of Hypocotyl Growth in Arabidopsis thaliana. *Plant Physiol.* **114**, 295–305 (1997).

20. A. M. Middleton, *et al.*, Mathematical modeling elucidates the role of transcriptional feedback in gibberellin signaling. *Proc. Natl. Acad. Sci.* **109**, 7571–7576 (2012).

21. A. Rizza, *et al.*, Differential biosynthesis and cellular permeability explain longitudinal gibberellin gradients in growing roots. *Proc National Acad Sci* **118**, e1921960118 (2021).

22. J. Griffiths, A. Rizza, B. Tang, W. B. Frommer, A. M. Jones, GIBBERELLIN PERCEPTION SENSOR 2 reveals genesis and role of cellular GA dynamics in light-regulated hypocotyl growth. *Plant Cell* **36**, 4426–4441 (2024).

23. A. Khakhar, *et al.*, ViparíNama: RNA viral vectors to rapidly elucidate the relationship between gene expression and phenotype. *Plant Physiol* 2020.06.03.130179 (2021). https://doi.org/10.1093/plphys/kiab197.

24. S. Lv, D. Yu, Q. Sun, J. Jiang, Activation of gibberellin 20-oxidase 2 undermines auxin-dependent root and root hair growth in NaCl-stressed Arabidopsis seedlings. *Plant Growth Regul* 1–12 (2017). https://doi.org/10.1007/s10725-017-0333-9.

25. J. Griffiths, *et al.*, Genetic Characterization and Functional Analysis of the GID1 Gibberellin Receptors in Arabidopsis. *Plant Cell Online* **18**, 3399–3414 (2006).

26. M. Ueguchi-Tanaka, *et al.*, GIBBERELLIN INSENSITIVE DWARF1 encodes a soluble receptor for gibberellin. *Nature* **437**, 693 (2005).

27. K. Murase, Y. Hirano, T. Sun, T. Hakoshima, Gibberellin-induced DELLA recognition by the gibberellin receptor GID1. *Nature* **456**, 459–463 (2008).

28. E. Shani, P. Hedden, T. Sun, Highlights in gibberellin research: A tale of the dwarf and the slender. *Plant Physiol.* kiae044 (2024). https://doi.org/10.1093/plphys/kiae044.

29. N. Illouz-Eliaz, *et al.*, Multiple Gibberellin Receptors Contribute to Phenotypic Stability under Changing Environments. *Plant Cell* **31**, 1506–1519 (2019).

30. A. Serrano-Mislata, *et al.*, DELLA genes restrict inflorescence meristem function independently of plant height. *Nature Plants* **3**, 749 (2017).

31. L. Hamama, *et al.*, Overexpression of RoDELLA impacts the height, branching, and flowering behaviour of Pelargonium × domesticum transgenic plants. *Plant Cell Rep* **31**, 2015–2029 (2012).

32. S. Jasinski, *et al.*, PROCERA encodes a DELLA protein that mediates control of dissected leaf form in tomato. *Plant J Cell Mol Biology* **56**, 603–12 (2008).

33. G. W. Bassel, R. T. Mullen, J. D. Bewley, procera is a putative DELLA mutant in tomato (Solanum lycopersicum): effects on the seed and vegetative plant. *J Exp Bot* **59**, 585–593 (2008).

34. L. Tomlinson, *et al.*, Using CRISPR/Cas9 genome editing in tomato to create a gibberellin-responsive dominant dwarf DELLA allele. *Plant Biotechnol J* **17**, 132–140 (2019).

35. A. M. Middleton, *et al.*, Mathematical modeling elucidates the role of transcriptional feedback in gibberellin signaling. *Proc. Natl. Acad. Sci.* **109**, 7571–7576 (2012).

36. J.-M. Davière, P. Achard, A Pivotal Role of DELLAs in Regulating Multiple Hormone Signals. *Mol Plant* **9**, 10–20 (2016).

37. A. Khakhar, A. R. Leydon, A. C. Lemmex, E. Klavins, J. L. Nemhauser, Synthetic hormone-responsive transcription factors can monitor and re-program plant development. *Elife* **7**, e34702 (2018).

38. S. Kiani, *et al.*, Cas9 gRNA engineering for genome editing, activation and repression. *Nat. Methods* **12**, 1051–1054 (2015).

39. J. Zalatan, M. Lee, R. Almeida, L. Gilbert, Engineering Complex Synthetic Transcriptional Programs with CRISPR RNA Scaffolds. (2015). https://doi.org/10.1016/j.cell.2014.11.052.

40. M. V. Arana, N. M. la Rosa, J. N. Maloof, M. A. Blázquez, D. Alabadí, Circadian oscillation of gibberellin signaling in Arabidopsis. *Proc. Natl. Acad. Sci.* **108**, 9292–9297 (2011).

41. R. J. Cowling, N. P. Harberd, Gibberellins control Arabidopsis hypocotyl growth via regulation of cellular elongation. *J. Exp. Bot.* **50**, 1351–1357 (1999).

42. T. Miao, *et al.*, Gibberellin regulates UV-B-induced hypocotyl growth inhibition in Arabidopsis thaliana. *Plant Signal. Behav.* **16**, 1966587 (2021).

43. N. Gonzalez, H. Vanhaeren, D. Inzé, Leaf size control: complex coordination of cell division and expansion. *Trends Plant Sci.* **17**, 332–340 (2012).

44. C.-T. Kwon, *et al.*, Rapid customization of Solanaceae fruit crops for urban agriculture. *Nat Biotechnol* **38**, 182–188 (2019).

45. N. Bouré, N. Arnaud, Molecular GA pathways as conserved integrators for adaptive responses. *Plant Biol.* **25**, 649–660 (2023).

46. F. Vandenbussche, A. C. Fierro, G. Wiedemann, R. Reski, D. V. D. Straeten, Evolutionary conservation of plant gibberellin signalling pathway components. *BMC Plant Biol.* **7**, 65 (2007).

47. A. Dill, T. Sun, Synergistic Derepression of Gibberellin Signaling by Removing RGA and GAI Function in Arabidopsis thaliana. *Genetics* **159**, 777–785 (2001).

48. C. Zhang, *et al.*, Gibberellin signaling modulates flowering via the DELLA–BRAHMA–NF-YC module in Arabidopsis. *Plant Cell* **35**, 3470–3484 (2023).

49. E. Weber, C. Engler, R. Gruetzner, S. Werner, S. Marillonnet, A Modular Cloning System for Standardized Assembly of Multigene Constructs. *PLoS ONE* **6**, e16765 (2011).

50. C. Engler, S. Marillonnet, DNA Cloning and Assembly Methods. *Methods Mol. Biol.* **1116**, 119–131 (2013).

51. K. Labun, *et al.*, CHOPCHOP v3: expanding the CRISPR web toolbox beyond genome editing. *Nucleic Acids Res.* **47**, W171–W174 (2019).

52. G. Pothoulakis, M. T. A. Nguyen, E. S. Andersen, Utilizing RNA origami scaffolds in Saccharomyces cerevisiae for dCas9-mediated transcriptional control. *Nucleic Acids Res.* **50**, 7176–7187 (2022).

53. S. J. Clough, A. F. Bent, Floral dip: a simplified method for Agrobacterium -mediated transformation of Arabidopsis thaliana. *Plant J.* **16**, 735–743 (1998).

54. T. Murashige, F. Skoog, A Revised Medium for Rapid Growth and Bio Assays with Tobacco Tissue Cultures. *Physiologia Plantarum* (1962).

55. D. C. Rio, M. Ares, G. J. Hannon, T. W. Nilsen, Purification of RNA Using TRIzol (TRI Reagent). *Cold Spring Harb. Protoc.* **2010**, pdb.prot5439 (2010).

56. M. L. Waskon, seaborn: statistical data visualization. *The Journal of Open Source Software* (2021). https://doi.org/10.21105/joss.03021.

Figures and Tables

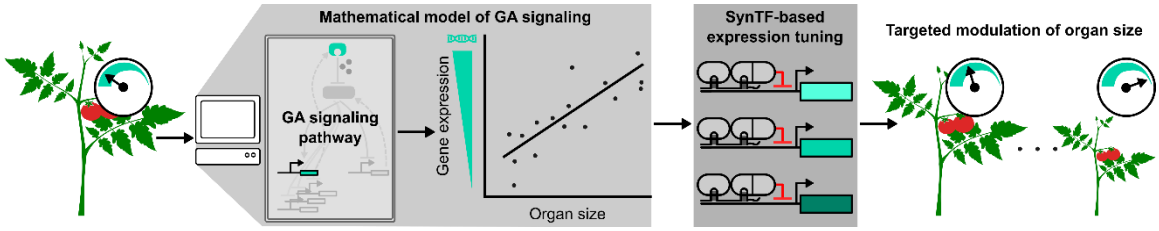

Figure 1. Graphical Abstract. This schematic lays out how we use mathematical modeling to guide synthetic transcription factor-based titration of gibberellin signaling gene expression and elucidate the design principles for predictably engineering organ size.

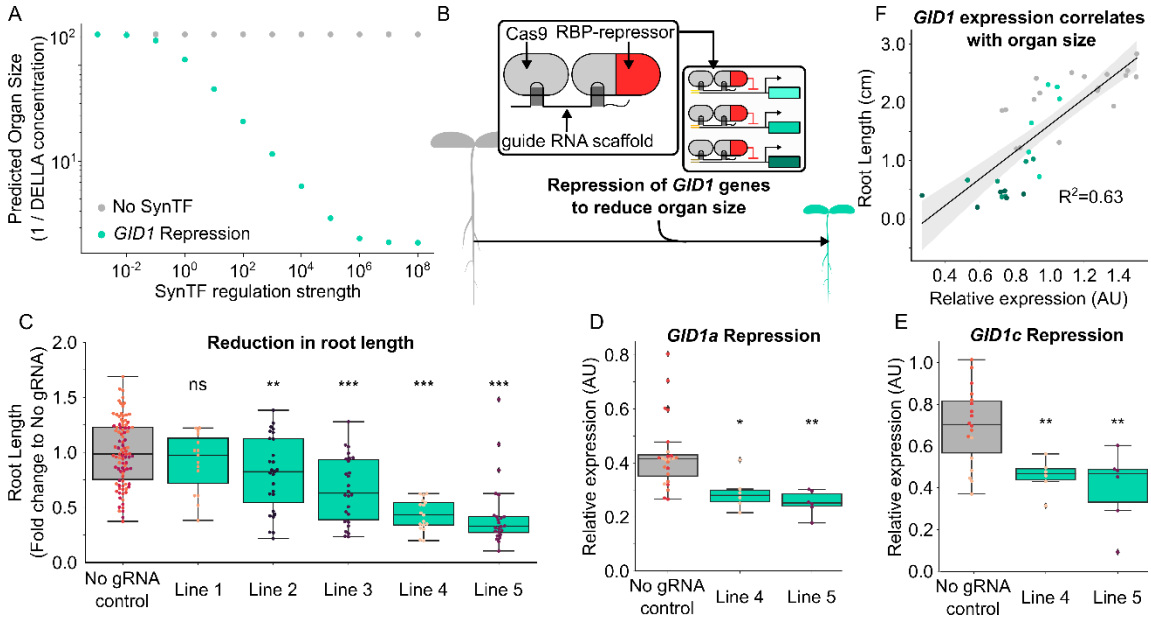

Figure 2. SynTF-based repression of *GID1* generates dose dependent dwarfing predicted via modeling in *A. thaliana.* A) Plot summarizing the predicted reciprocal of DELLA protein concentration at steady state, used as a proxy for organ size, from simulations of the GA signaling network with either No SynTF (grey) or a repressor targeted to regulate *GID1* (teal), across a range of different SynTF regulation strengths. B) A schematic of the Cas9-based synthetic transcription factor used to implement repression on the three different *GID1* homologs in *A. thaliana* which is predicted to decrease organ size. C) Boxplots summarizing the fold change in root length of plant lines with SynTF-based repression of *GID1* (teal) compared to a population of no gRNA control plant lines (n=4) (gray). Every dot of the same color corresponds to an independent biological replicate of the same genotype. Ns stands for non-significant, ** corresponds to $p < 0.005$, and *** corresponds to $p<0.0005$. D,E) Boxplots summarizing the expression of *GID1a* (D) and *GID1c* (E) normalized by housekeeping gene expression in seedlings of a population of either no gRNA control lines (gray, n=3) or the *GID1* repression lines with the strongest phenotypes (teal). Every dot of the same color corresponds to an independent biological replicate of the same genotype, * corresponds to $p < 0.05$, and ** corresponds to $p<0.005$. F) Scatter plot that demonstrates the correlation (R^2=0.63) between root length and the sum of normalized *GID1a* and *GID1c* expression. Every dot of the same color corresponds to an independent biological replicate of either the no gRNA control lines (gray) or *GID1* repression lines 1, 4, and 5 (progressively darker shades of teal).

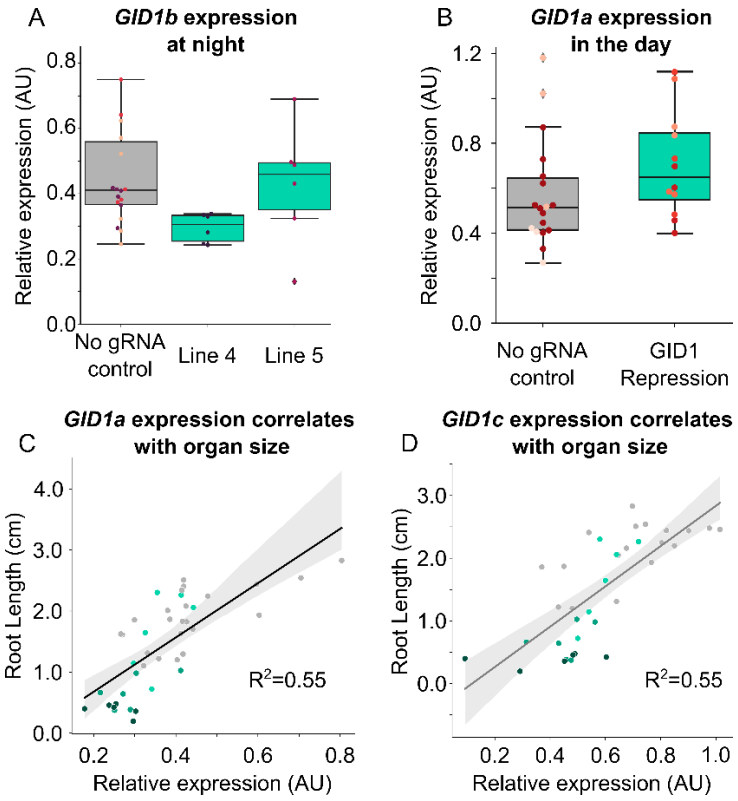

Supplementary Figure S1. A) Boxplots summarizing the expression of *GID1b* normalized by housekeeping gene expression in seedlings of a population of no gRNA control lines (gray, n=3) and the *GID1* repression lines with the strongest phenotypes (teal). Every dot of the same color corresponds to an independent biological replicate of the same genotype. B) Boxplots summarizing the expression of *GID1a* normalized by housekeeping gene expression in seedlings whose tissue was collected in the day rather than in the evening as in Fig. 1, from a population of no gRNA control lines (gray, n=3) and the *GID1* repression lines with the strongest phenotypes (teal). Every dot of the same color corresponds to an independent biological replicate of the same genotype. C,D) Scatter plots that depict the correlation between root length and normalized *GID1a* (C, R^2=0.55) and *GID1c* (D, R^2=0.55) expression. Every dot of the same color corresponds to an independent biological replicate of either the no gRNA control lines (gray) or *GID1* repression lines 1, 4, and 5 (progressively darker shades of teal).

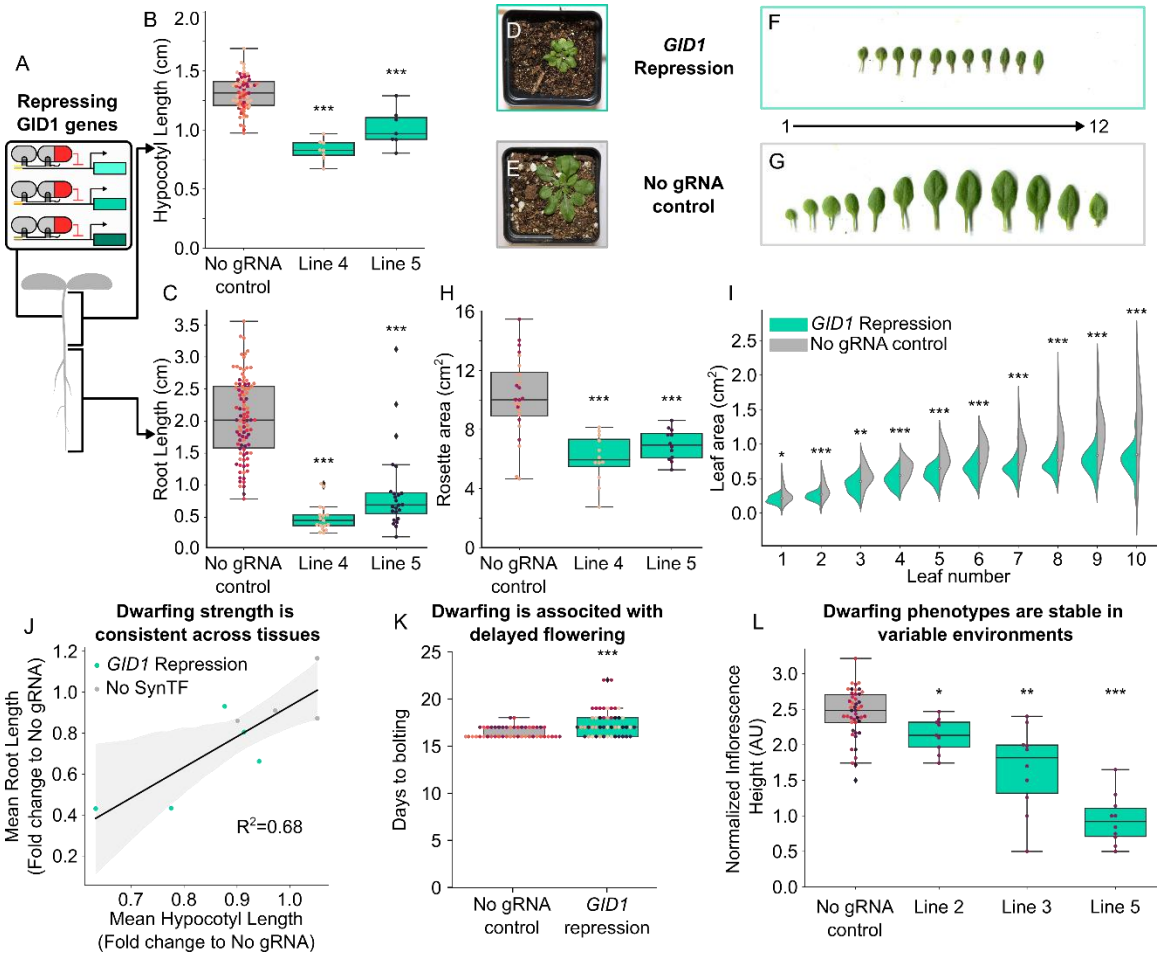

Figure 3. SynTF-based *GID1* repression generates consistent dwarfing across tissues and environments. A) Cartoon depicting the genetic circuit enabling SynTF-based repression of *GID1* genes and highlighting the portions of *A. thaliana* seedlings measured to record organ size. B,C) Boxplots summarizing hypocotyl length (B) and primary root length (C) of the two *GID1* repression lines that had the strongest dwarfing phenotypes (teal) compared to a population of no gRNA control plant lines (n=4) (gray). D,E,F,G) Representative pictures of rosettes (D,E) and dissected leaves arranged according to developmental age (F,G) from *GID1* repression (teal), and no gRNA control lines (grey), respectively. H) Boxplots summarizing the total rosette leaf area of the two plant lines with SynTF-based repression of *GID1* (teal) compared to a population of no gRNA control plant lines (gray, n=3). I) Stacked violin plot showing distribution of leaf areas for plant lines with SynTF-based repression of *GID1* (teal, 3 lines with 10 biological replicates) compared to No gRNA control plant lines (gray, 2 lines with 10 biological replicates) for each leaf in developmental time where leaf 10 is youngest measured. K) Boxplots summarizing the height of inflorescences normalized by the number of days post bolting of plant lines with SynTF-based repression of *GID1* (teal) compared to a population of No gRNA control plant lines (gray, n=3) grown in a variable greenhouse environment. Across all boxplots every dot of the same color corresponds to an independent biological

replicate of the same genotype, * corresponds to $p < 0.05$, ** corresponds to $p < 0.005$, and *** corresponds to $p<0.0005$.

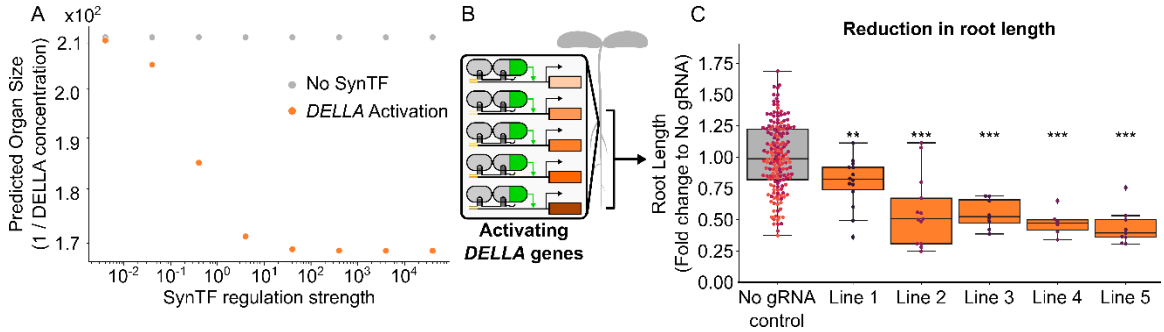

Figure 4. SynTF-based activation of DELLA genes also generates model-predicted dwarfing. A) Plot summarizing the predicted reciprocal of DELLA protein concentration at steady state, used as a proxy for organ size, from simulations of the GA signaling network with either no SynTF (grey) or an activator targeted to regulate *DELLA* genes (orange), across a range of different SynTF regulation strengths. B) Schematic of the genetic circuit designed to implement SynTF-based activation on five *DELLA* homologs in *A. thaliana*. C) Boxplots summarizing the fold change in root length of plant lines with SynTF-based activation of DELLA expression (orange) compared to a population of no gRNA control plant lines (n=4) (gray). Across all boxplots, every dot of the same color corresponds to an independent biological replicate of the same genotype, ** corresponds to $p < 0.005$, and *** corresponds to $p<0.0005$.

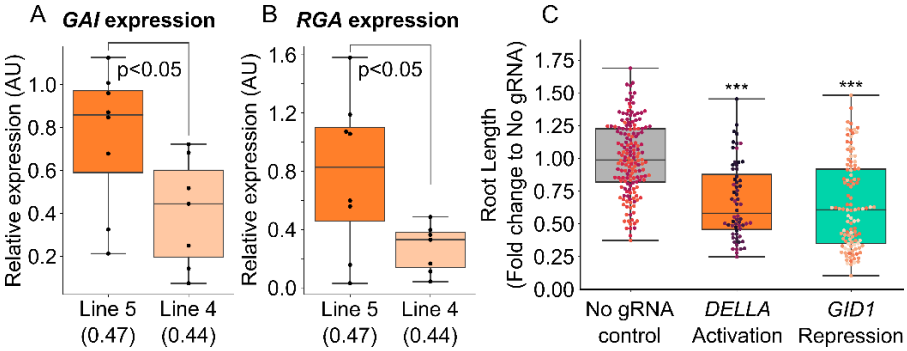

Supplementary Figure S2. A,B) Boxplots summarizing significant differences in relative expression of both *GAI* (A) and *RGA* (B) in two *DELLA* activation lines, namely Line 5 (0.47 fold decrease in root length compared to no guide control, dark orange) and Line 4 (0.44 fold decrease in root length compared to no guide control, light orange). Each dot represents an independent biological replicate. C) Boxplots comparing the relative difference in fold change of root length across plant lines with either SynTF-based repression of *GID1* expression (teal, n=5) or SynTF-based activation of *DELLA* expression (orange, n=5) to a population of no gRNA control plant lines (grey, n=4). *** corresponds to p<0.0005.

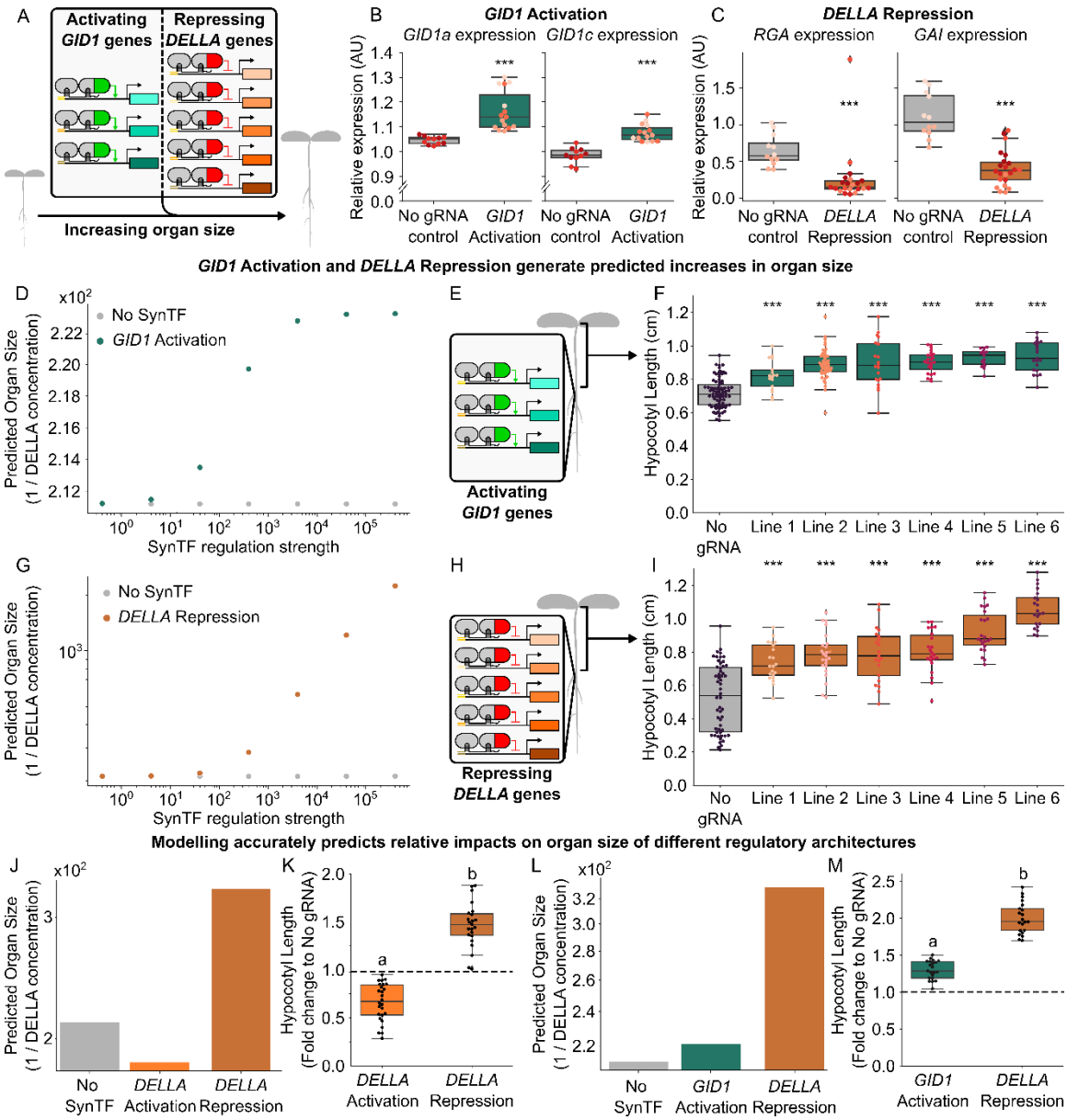

Figure 5. Models of SynTF modulation of GA signaling correctly predict that repression of *DELLA* expression generates larger increases in organ size than activation of *GID1*. A) Schematic describing genetic circuits designed to either activate *GID1* expression or repress *DELLA* expression to increase organ size. B,C) Boxplots summarizing the expression of *GID1a* and *GID1c* (B) or *RGA* and *GAI* (C) normalized by housekeeping gene expression in seedlings of a population of no gRNA control lines (gray, n=2) and either *GID1* activation lines (B, dark teal, n=3) or *DELLA* repression lines (C, dark orange, n=3). Every dot of the same color corresponds to an independent biological replicate of the same genotype and *** corresponds to p<0.0005. D,G) Plots summarizing the predicted reciprocal of DELLA protein concentration at steady state, used as a proxy for organ size,

from simulations of the GA signaling network with either no SynTF (grey), an activator targeted to regulate *GID1* expression (D, dark teal), or a repressor targeted to regulate *DELLA* expression (G, dark orange) across a range of different SynTF regulation strengths. E,H) Schematic of the genetic circuit designed to implement either SynTF-based activation on the three *GID1* homologs (E) or SynTF-based repression on the five *DELLA* homologs (H) in *A. thaliana*. F,I) Boxplots summarizing the hypocotyl length of plant lines with either SynTF-based activation of *GID1* expression (dark teal, F) or SynTF-based repression of *DELLA* (dark orange, I) compared to a population of no gRNA control plant lines (n=4, gray). Across all boxplots, every dot of the same color corresponds to an independent biological and *** corresponds to $p<0.0005$. J) Bar plots summarizing the predicted reciprocal of DELLA protein concentration at steady state, used as a proxy for organ size, from simulations of the GA signaling network with either no SynTF (grey), an activator targeted to regulate *DELLA* expression (orange), or a repressor targeted to regulate *DELLA* expression (dark orange). K) Boxplots summarizing the fold change in hypocotyl length compared to the no gRNA controls of the *DELLA* activation (orange) or *DELLA* repression (dark orange) line with the strongest phenotype. The dashed black line highlights the phenotype of the no gRNA control. Every dot of the same color corresponds to an independent biological replicate and the letters above plots correspond to significantly different group based on a one-way ANOVA test. L) Bar plots summarizing the predicted reciprocal of DELLA protein concentration at steady state, used as a proxy for organ size, from simulations of the GA signaling network with either no SynTF (grey), an activator targeted to regulate *GID1* (dark teal) expression, or a repressor targeted to regulate DELLA expression (dark orange). M) Boxplots summarizing the fold change in hypocotyl length compared to the no gRNA controls of the *DELLA* repression (dark orange) or *GID1* activation (dark teal) line with the strongest phenotype. The dashed black line highlights the phenotype of the no gRNA control. Every dot of the same color corresponds to an independent biological replicate and the letters above plots correspond to significantly different group based on a one-way ANOVA test.

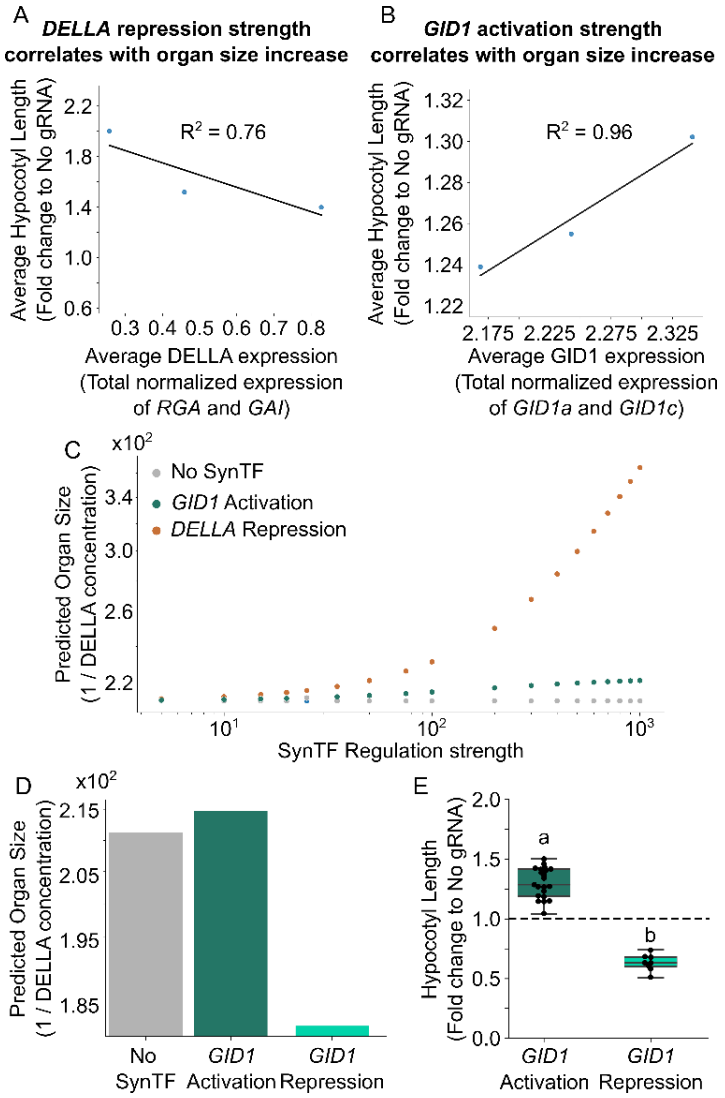

Supplementary Figure S3. A) Scatter plot that demonstrates the correlation (R^2=0.76) between average fold change in hypocotyl length compared to the no gRNA controls and the average sum of normalized *RGA* and *GAI* expression across three *DELLA* repression lines. Each dot represents an independent plant line. B) Scatter plot that demonstrates the correlation (R^2=0.96) between average fold change in hypocotyl length compared to no gRNA controls and the average sum of normalized *GID1a* and *GID1c* expression across three *GID1* activation lines. Each dot represents an independent plant line. C) Plots summarizing the predicted reciprocal of *DELLA* protein concentration at steady state, used as a proxy for organ size, from simulations of the GA signaling network with either no SynTF (grey), an activator targeted to regulate *GID1* expression (dark teal), or a repressor targeted to regulate *DELLA* expression (dark orange) across a range of different SynTF regulation strengths. D) Bar plots summarizing the predicted reciprocal of DELLA protein concentration at steady state, used as a proxy for organ size, from simulations of the GA signaling network with either no SynTF (grey), an activator targeted to regulate *GID1* expression (dark teal), or a repressor targeted to regulate *GID1* expression (teal). E)

Boxplots summarizing the fold change in hypocotyl length compared to no gRNA controls of the *GID1* repression (teal) or *GID1* activation (dark teal) line with the strongest phenotype. The dashed black line highlights the phenotype of the no gRNA control. Every dot of the same color corresponds to an independent biological replicate and the letters above plots correspond to significantly different group based on a one-way ANOVA test.

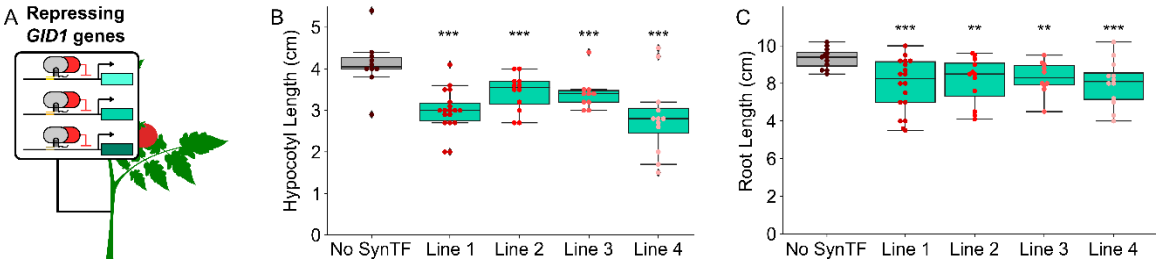

Figure 6. Repression of GID1 generates consistent dwarfing across tissues in tomato. A) A schematic of the Cas9-based synthetic transcription factor used to implement repression on the three different GID1 homologs in *S. lycopersicum* (tomato) which is predicted to decrease organ size. B,C) Boxplots summarizing hypocotyl length (B) and root length (C) of four independent plant lines with SynTF-based repression of GID1 (teal) compared to a control plant line lacking the SynTF (gray). Every dot of the same color corresponds to an independent biological replicate of the same genotype, ** corresponds to $p < 0.005$, and *** corresponds to $p<0.0005$.

Supplemental Table S1. List of plasmids.

Plasmid #	Plasmid Description	Link to Annotated Plasmid Maps
P210	pMOD_B_pGmUbi:NLS-MCP-DREB2A-tUBQ1	https://benchling.com/s/seq-MwAvZNSQJKqmA7jjQk1k?m=slm-ZNVOkLxETBFbsCeVuaIr
P218	pMOD_C_p35s:NLS-PCP-TPLN300:tNos	https://benchling.com/s/seq-oeZenFJYD4aXba0VMmo1?m=slm-LaJYSfMpSU2n9dshIt84
P251	pMOD_D-p35s:AtDELLA_guides1-1xMS2:t35s	https://benchling.com/s/seq-34IAd2Ak7qPAOPtTvCAs?m=slm-w694bkGtyaDy3b5zhTb7
P387	pMOD_A_pUBQ10:NLS-Cas9-tHSP	https://benchling.com/s/seq-gcG6pGbgeOKdE49GSFEO?m=slm-TdLwqOoOyOaqvvucPXE7
P671	pTRANS_220d-pUBQ10:NLS-AtCas9:tHSP - pGmUbi:NLS-MCP-DREB2A-tUBQ1 - p35s:NLS-PCP-TPLN300:tNos - p35s:AtDELLA_guides1-1xMS2:t35s	https://benchling.com/s/seq-mma2v82CeUQxRfDfBdVF?m=slm-KRvmsgJFG25S8quBPrvg
P683	pTRANS_220d-pUBQ10:NLS-AtCas9:tHSP - pGmUbi:NLS-MCP-DREB2A-tUBQ1 - p35s:NLS-PCP-TPLN300:tNos - p35s:AtGID_guides1-1xPP7:t35s	https://benchling.com/s/seq-qKv521SztV10SKaIMc3t?m=slm-oeJhMAjbWFHnsnHL3gZM
P684	pTRANS_220d-pUBQ10:NLS-AtCas9:tHSP - pGmUbi:NLS-MCP-DREB2A-tUBQ1 - p35s:NLS-PCP-TPLN300:tNos - p35s:AtGID_guides1-2xPP7:t35s	https://benchling.com/s/seq-vYJisQVdibhGCT1twsBJ?m=slm-ntsZ2SOAqxoahDdTzp3M
P710	pMOD_D-p35s:DELLA-guides-2xPP7-t35s	https://benchling.com/s/seq-25g28HyVAIDdktL1qIL6?m=slm-BhxFy2z7oIobWEfciyLU
P731	PMOD_D-p35s:GID-guides-1xMS2-t35s	https://benchling.com/s/seq-e67WY9o1PfYe5VvBaZ1F?m=slm-z2sjl8sWoZKQMWHFALMf
P735	pMOD_D1'-p35s:AtGID_guides1-1xPP7	https://benchling.com/s/seq-qU5SNDnPoYaabhH75pW3?m=slm-b9VXW7CuCIAoAtOI9HHz
P768	pMOD_D1'-p35s:AtGID_guides1-2xPP7	https://benchling.com/s/seq-l7vxkJhLRhQarZoLSi27?m=slm-5Q9ARa1MZtOApbqkLY9Z
P860	pMOD_D2'-p35s:AtGID_guides2-1xPP7	https://benchling.com/s/seq-cgas2gwIwy4O9YwY30Ll?m=slm-DS2ZnZas1snmImWMcFVU
P861	pMOD_D2'-p35s:AtGID_guides2-2xPP7	https://benchling.com/s/seq-4dU0OooeiqPd5ZYSpY3H?m=slm-Q5io5eJT02jhiNgEgPAY

Plasmid #	Plasmid Description	Link to Annotated Plasmid Maps
P925	pTRANS_220d-pUBQ10:NLS-Cas9-tHSP-pGmUbi:NLS-MCP-DREB2A-tUBQ1-p35s:NLS-PCP-TPLN300:tNos-p35s:GID-guides1-2xPP7-t35s - p35s:GID-guides2-2xPP7-t35s	https://benchling.com/s/seq-rbcGB2xbNlubWVsh031c?m=slm-SgAUseEU9cvW8lpwaW2Z
P1212	pTRANS_220d-pUBQ10:NLS-Cas9-tHSP-pGmUbi:NLS-MCP-DREB2A-tUBQ1-NLS-PCP-TPLN300:tNos-p35s:DELLA-guides-2xPP7-t35s	https://benchling.com/s/seq-Szsa9qRgv2rZRLKGh51F?m=slm-2bd96Ox94IZwMRabNePn
P1317	pTRANS_220d-pUBQ10:NLS-Cas9-tHSP-pGmUbi:NLS-MCP-DREB2A-tUBQ1-p35s:NLS-PCP-TPLN300:tNos-p35s:GID-guides-1xMS2-t35s	https://benchling.com/s/seq-Obu7yyCpOC9QV0nPTKPB?m=slm-5hF50ttCvqTvwuyMuBnI

Supplemental Table S2. List of sequences targeted by sgRNAs.

Guide name	Sequence (3' to 5')
GID1a_Target1	AGGGATGAGTAGGG
GID1a_Target2	TGTTGGGTCATGGG
GID1a_Target3	TGCGCGCATAAGTT
GID1a_Target5	GGATAAACAACAAA
GID1a_Target6	GTCAATTTTATTCG
GID1b_Target1	GACCAATCGGACGG
GID1b_Target2	TACACATGACACCG
GID1b_Target3	AGCACTAATGAGAG
GID1b_Target5	GAATTAGGAAGCAG
GID1b_Target6	GAATTAGGAAGCAG
GID1c_Target1	AAGAATATCGGCGT
GID1c_Target2	CGACTGTTGTTGGG
GID1c_Target3	TGCGAACAGATTAA
GID1c_Target5	TCAGAATACTAGAA
GID1c_Target6	CACCCTTGGGAGCA
RGA_Target1	CATCTAAAGTGATA
GAI_Target1	TGTCATGCAACTAG
RGL1_Target1	TTGCGGTTGTACCA
RGL2_Target1	TTCTTAAACCCAAA
RGL3_Target1	CGGGCTGTTACTTT

Supplemental Table S3. List of primers.

Primer Name	Primer Sequence (5' to 3')	Use
AtGID1A qPCR f	GGCTCAAGAAAGCGGGTCAAGAG	RT-qPCR

AtGID1A qPCR r	GCGTTTACAAACGCCGAAATCTCATCC	RT-qPCR
AtGID1b_qPCR-f	ATGTTTGGTGGACAGGAGAG	RT-qPCR
AtGID1b_qPCR-r	CGGTAGATAAGCCCTCCAATAC	RT-qPCR
AtGID1c_qPCR-f	GTTTGGAGGGACCGAAAGAA	RT-qPCR
AtGID1c_qPCR-r	AGGAAGAAACGCTCTCCAATAC	RT-qPCR
PP2A_q-f	AACGTGGCCAAAATGATGC	RT-qPCR
PP2A_q-r	AACCGCTTGGTCGACTATCG	RT-qPCR
qPCR SlGID1ac-f	GGACTCGAAGGCTCACATATAC	RT-qPCR
qPCR SlGID1ac-r	TGGATTCTACTGCCCTGAAAG	RT-qPCR
qPCR_SlGID1b-1-f	ACATTCTGTCGTCGTCTTGTT	RT-qPCR
qPCR_SlGID1b-1-r	GCAGCCCATCCATCATCATA	RT-qPCR
qCAC-f	CCTCCGTTGTGATGTAACTGG	RT-qPCR
qCAC-r	ATTGGTGGAAAGTAACATCATCG	RT-qPCR
GID1a_exon1toexon2_junction-f	CACTTCTCGACTTGCAAATTC	PCR to check gDNA contamination
GID1a_exon1toexon2_junction-r	ATTGTAGGCTACTTTGAAGTTGG	PCR to check gDNA contamination
AtRGA1 qPCR-f	CGCAGATTGGTGGAGTCATAG	RT-qPCR
AtRGA1 qPCR-r	CTTGCGAGTCAACCAGGATAA	RT-qPCR
AtGAI qPCR-f	CTATGCTCACCGACCTTAATCC	RT-qPCR
AtGAI qPCR-r	GACGAAGAAGCCGAATCGATAG	RT-qPCR

Supplemental Table S4. Gene accessions referenced in the manuscript.

Gene Name	**Accession No.**	**Species**
GID1a	AT3G05120	*Arabidopsis thaliana*
GID1b	AT3G63010	*Arabidopsis thaliana*
GID1c	AT5G27320	*Arabidopsis thaliana*
GAI	AT1G14920	*Arabidopsis thaliana*
RGA	AT2G01570	*Arabidopsis thaliana*
RGL1	AT1G66350	*Arabidopsis thaliana*
RGL2	AT3G03450	*Arabidopsis thaliana*
RGL3	AT5G17490	*Arabidopsis thaliana*
GID1a	Solyc01g098390	*Solanum lycopersicum*
GID1b1	Solyc09g074270	*Solanum lycopersicum*
GID1b2	Solyc06g008870	*Solanum lycopersicum*